ROYAL SOCIETY
OF CHEMISTRY

PAPER

Check for updates

Hierarchical mesoporous NanoMUV-2 for the selective delivery of macromolecular drugs†

Isabel Abánades Lázaro, [iD] * María Vicent-Morales, [iD]
Guillermo Mínguez Espallargas [iD] and Mónica Giménez-Marqués [iD] *

Although Metal–organic frameworks (MOFs) have received attention as drug delivery systems, their application in the delivery of macromolecules is limited by their pore size and opening. Herein, we present the synthesis of nanostructured MUV-2, a hierarchical mesoporous iron-based MOF that can store high payloads of the macromolecular drug paclitaxel (*ca.* 23% w/w), increasing its selectivity towards HeLa cancer cells over HEK non-cancerous cells. Moreover, this NanoMUV-2 permits full degradation under simulated physiological conditions while maintaining biocompatibility, and is amenable to specific surface modifications that increase its cell permeation, efficient cytosol delivery and cancer-targeting effect, further intensifying the cancer selectivity of paclitaxel.

Introduction

Metal–organic frameworks (MOFs)[1,2] have received notable attention as drug delivery systems,[3–6] as these porous crystalline hybrid solids can store high drug payloads,[7,8] enhancing their pharmacokinetics and reducing their side effects. Moreover, the virtually infinite choice of metal and ligands enables fine-tuning of their structure, serving as efficient platforms to incorporate targeting units,[9,10] responsive polymers,[11,12] and even imaging components for theragnostic purposes,[13,14] while remaining biocompatible.[15–17] Nevertheless, the application of MOFs for the delivery of specific large biomolecules is limited by their pore size and window opening and the ease of *in situ* formation.[18,19]

Paclitaxel (PTX), with a molecular size of *ca.* $18 \times 15 \times 8$ Å^3, is one of the most effective chemotherapeutics,[20] but due to its reduced solubility, its commercial form, Taxol, has associated side effects[21] that have led to the urgency of finding alternative formulations.[22,23] MOFs have been considered as encapsulating PTX materials, but given the notable molecular size of this drug, the number of reported studies of PTX@MOF formulations remains limited.[24–27] For instance, theoretical studies have reported that PTX can only be loaded into Zr-bdc (UiO-66) if defective regions of missing clusters are present.[28]

To overcome the size limitation, mesoporous MOFs such as Zn-BPDC and Zn-azoBPDC,[29] and the Fe-TCPP PCN-600,[30] have been studied. However, despite these recent advances in MOF-

based PTX formulations, direct evidence of PTX pore loading remains elusive and more importantly, a deficient therapeutic effect prevails as compared with the free-administered drug. Therefore, the development of new PTX@MOF formulations, including a comprehensive study of the composite nature, is desired to improve PTX therapeutic performance.

MUV-2 (MUV stands for materials of the University of Valencia), represented in Fig. 1a, is an stable iron-based mesoporous MOF built from the self-assembly of $[Fe_3(\mu_3\text{-}O)(COO)_6]$ clusters and tetratopic tetrathiafulvalene tetrabenzoic acid (H_4TTFTB) ligands forming a 3,6-connected network with **ttp** topology and formula $(TTFTB)_3[(Fe_3O)(H_2O)_2(OH)]_2$.[31] This hierarchical mesoporous MOF, with *ca.* 80% of calculated free volume, displays 1D hexagonal channels of *ca.* 3 nm and orthogonal microporous channels of *ca.* 1 nm.[31–33] Despite exhibiting optimal biocompatible composition, MUV-2 has not been reported for drug delivery applications, mainly due to a lack of development in MOF miniaturization. Thus, we postulate that the development of mesoporous NanoMUV-2 shall be suitable for the storage and effective release of macromolecules such as PTX.

Herein, we present a comprehensive study of NanoMUV-2 as a PTX delivery system, thoroughly evaluating its colloidal and physiological stabilities, cellular internalization, surface modification and the effect of these variables on selective PTX delivery to cancer cells.

Results and discussion

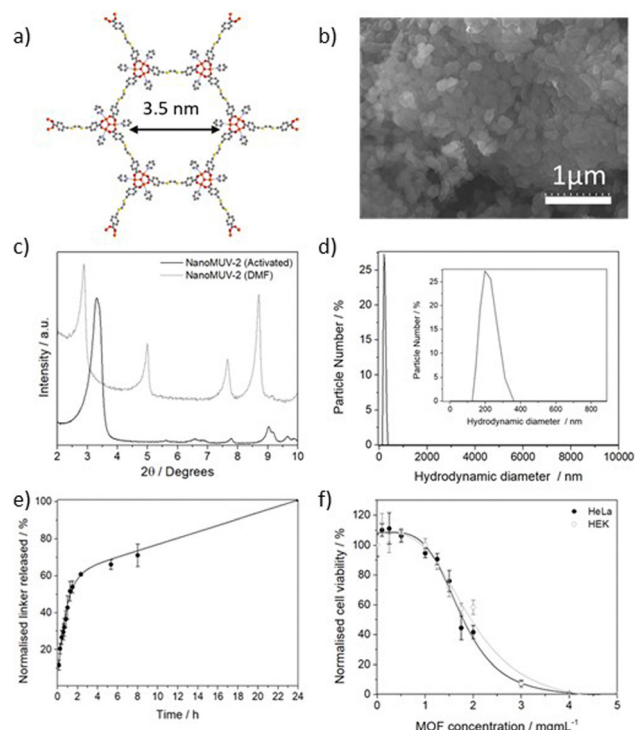### NanoMUV-2 and its colloidal and physiological properties

The miniaturization of MUV-2 to the nanoscale was developed by fine-tuning the reported synthetic conditions.[31] Essentially,

Instituto de Ciencia Molecular (ICMol), Universitat de València, Catedrático José Beltrán Martínez No 2, 46980 Paterna, Valencia, Spain.
E-mail: isabel.abanades@uv.es, monica.gimenez-marques@uv.es

This journal is © The Royal Society of Chemistry 2023

J. Mater. Chem. B, 2023, **11**, 9179–9184 | **9179**

Fig. 1 (a) Schematic representation of MUV-2 structure, showing the hexagonal mesopores of 3.5 nm. (b) Scanning Electron Microscopy Image of NanoMUV-2 nanoparticles. (c) PXRD patterns of activated NanoMUV-2 (closed form) and NanoMUV-2 immersed in DMF (open form) revealing its breathing behavior. (d) Hydrodynamic diameter of NanoMUV-2 in PBS 10X obtained by DLS analysis. (e) Kinetic profile of linker release from NanoMUV-2 in PBS 10X. (f) HeLa and HEK cells' viability upon incubation with different concentrations of NanoMUV-2. Error bars represent the standard deviation of 3 independent experiments, each of them with $n = 4$.

reducing the quantity of acetic acid modulator toward a less acidic pH (see section S2 in the ESI†) should promote the nucleation and crystallization rates leading to a smaller particle size.[34] This resulted in homogeneous nanoparticles of 190 ± 59 nm, as determined by Scanning Electron Microscopy (SEM) (Fig. 1b). In contrast to other reported flexible MOFs,[35] NanoMUV-2 retains its breathing behavior, as demonstrated by the changes in the solvated and desolvated Powder X-Ray Diffraction (PXRD) patterns (Fig. 1c). The material was thoroughly washed with DMF and ethanol, with its complete

activation being confirmed by several characterisation techniques (see section S3 in the ESI† for detailed characterisation).

To assess the suitability of NanoMUV-2 for drug delivery applications, the colloidal stability of the activated material was evaluated by Dynamic Light Scattering (DLS) in phosphate-buffered saline (PBS) 10X medium. NanoMUV-2 dispersed well in PBS 10X, showing average hydrodynamic diameters of ca. 220 nm (Fig. 1d), similar to the particle size determined by SEM (190 ± 59 nm). The chemical stability of NanoMUV-2 in PBS 10X (pH = 7.4) was investigated by UV-Vis spectroscopic determination of linker release (H_4TTFTB). A fast degradation with a burst release of the linker occurs during the first 2 hours (ca. 60%), likely due to the high porosity and pore accessibility of NanoMUV-2, reaching complete degradation after 24 hours, as represented in Fig. 1e. This kinetic profile may be distinct under different PBS concentrations, for instance in cell growth media or the blood current, where MOFs are known to form a protein corona that prevents their degradation.[36,37]

Given the biocompatibility of its precursors, with the sodium salt of the ligand exhibiting a 50% inhibitory concentration (IC_{50}) after 72 hours of 0.64 ± 0.06 and 0.54 ± 0.05 mg mL^{-1} for cervix cancer HeLa and non-cancerous HEK cell lines respectively (see section S3.8 in the ESI†), we assessed the effect of NanoMUV-2 using the MTS assay (Fig. 1f). NanoMUV-2 exhibited optimal biocompatibility for both HeLa and HEK cell lines, with an IC_{50} of 1.92 ± 0.31 and 2.02 ± 0.32 mg mL^{-1} respectively, after 72 hours of incubation. In this regard, the IC_{50} of the maximum delivered ligand (corresponding to ca. 1.54 and 1.63 mg mL^{-1} of ligand, based on the molecular formula) is higher than the one of the free ligand salt in both cases, suggesting poor internalization and/or incomplete cytosol delivery.

Cellular internalisation of NanoMUV-2

To evaluate this possibility, we loaded NanoMUV-2 with calcein, a carboxylate-containing fluorescent molecule that cannot efficiently cross the cell membrane due to its hydrophilicity, making it an excellent proof for MOFs' internalization[38] (see section S4 in the ESI† for detailed characterisation). After extensive washing, calcein loading was determined to be $17.0 \pm 0.5\%$ w/w by UV-Vis and Thermo Gravimetic Analysis (TGA), whereas the resultant Cal@NanoMUV-2 retains its crystalline structure as determined by PXRD (Fig. 2a). N_2 sorption

Fig. 2 (a) PXRD pattern of Cal@NanoMUV-2 compared to NanoMUV-2 (activated). (b) Pore size distribution obtained from N_2 adsorption isotherms of Cal@NanoMUV-2 compared to NanoMUV-2 (activated). (c) Kinetics of calcein release from Cal@NanoMUV-2 in PBS 10X. (d) Normalized cytoplasmic fluorescence of HeLa and HEK cells upon incubation with different concentrations of free calcein and Cal@NanoMUV-2. Error bars represent the standard deviation of 3 independent experiments. The normalization is performed as fold-increase towards the untreated cells control.

9180 | J. Mater. Chem. B, 2023, 11, 9179–9184

This journal is © The Royal Society of Chemistry 2023

studies confirmed calcein loading into the pores, as deduced by analysis of the pore size distribution where the pores larger than calcein molecular size (13 Å)[39] were absent (Fig. 2b). Using calcein as a model drug[38] we measured its delivery in PBS 10X (Fig. 2c), revealing the expected fast release and completeness after 4 hours, in agreement with MOF degradation.

Flow-assisted cell sorting (FACS) was used to monitor the cellular internalization of Cal@NanoMUV-2 by HeLa cervix cancer and HEK non-cancerous cells (see section S5.1 in the ESI†). Between a 3- and 4-fold increase in calcein internalization was confirmed by FACS after 2 hours of incubation with free calcein and Cal@NanoMUV-2, which was consistent through different concentrations (Fig. 2d) and further confirmed by confocal microscopy (see section S5.2 in the ESI†). Comparison of normalized cytoplasmic fluorescence determined through FACS upon incubation with Cal@NanoMUV-2 at 37 °C and 4 °C indicates that the MOF is mainly internalized through active transport such as endocytosis. Interestingly, the normalized cytoplasmic fluorescence upon incubation with Cal@-NanoMUV-2 was slightly higher for HeLa than for HEK cells, ranging from 1.1- to 1.5-fold increase. Lysotracker was used to stain lysosomes and determine if Cal@NanoMUV-2 can undergo efficient calcein cytosol delivery.[40] Manders' colocalisation coefficients indicate high colocalisation of calcein and lysosomes for both HeLa and HEK cells, which is in agreement with the reduced effect on cell viability when compared to the free linker salt.

The exceptionally large pores of MUV-2 make it an interesting candidate for the delivery of macromolecular therapeutic agents such as PTX. Essentially, we loaded PTX into NanoMUV-2 by a simple impregnation method revealing ca. 22% w/w loading after extensive washing as determined by UV-Vis (see section S6 in the ESI†). PXRD confirmed the structural integrity of the resultant PTX@NanoMUV-2 composite material (Fig. 3a). As control studies, we evaluated the well-studied MIL-100(Fe)[5] and UiO-66(Zr)[3] MOFs for PTX delivery (see section S7 in the ESI†), confirming negligible PTX inclusion as expected for the molecular size limitation.[28] This was further confirmed by FT-IR and TGA,[41] where PTX features were observed only for MUV-2 and not for the other MOFs, with TGA revealing similar loadings (ca. 23% w/w) to UV-Vis determination (Fig. 3b).

Moreover, N_2 sorption analysis unequivocally confirmed the successful loading of PTX into NanoMUV-2 pores (see section S6 in the ESI†), as deduced from the pore size distribution analysis where the small mesopore contribution is reduced after loading together with a complete disappearance of pores ranging from 15.5 to 20.3 Å corresponding with the PTX molecular size ($18.2 \times 15.2 \times 7.9$ Å[3] (Fig. 3c).[20]

After confirmation of significant PTX pore loading, we evaluated the cytotoxic effect of PTX@NanoMUV-2 and free PTX in cervix cancer HeLa cells and non-cancerous HEK cells (Fig. 3d). PTX@NanoMUV-2 was less cytotoxic than free PTX towards both cell lines, in agreement with partial lysosome colocalisation, but its anticancer selectivity was slightly increased (see section S8 in the ESI†), possibly due to the enhanced internalization of cancer cells. At low concentrations (0.02 mg mL^{-1} of MOF, corresponding to a maximum delivery

Fig. 3 (a) PXRD pattern of PTX@NanoMUV-2 compared to NanoMUV-2 (activated). (b) TGA profiles of PTX@NanoMUV-2 compared to NanoMUV-2 (activated). (c) Pore size distribution obtained from N_2 adsorption isotherms of PTX@NanoMUV-2 compared to NanoMUV-2 (activated). (d) HeLa and HEK cells' viability upon incubation with different concentrations of free PTX and PTX@NanoMUV-2 as a function of the maximum PTX concentration that could be delivered by the MOFs. Error bars represent the standard deviation of 3 independent experiments, each of them with $n = 4$.

of PTX of ca. 4.4 μg mL^{-1} as represented in Fig. 3d), PTX@Na-noMUV-2 reduced HeLa cells' proliferation to 60 ± 9% cell viability, but had no negative effect on HEK cells (119 ± 6% cell viability), whereas for a concentration of 4 μg mL^{-1} of free Taxol, HeLa cells' viability is reduced to 19 ± 6% and HEK cells to 42 ± 5%. Calculating the anticancer selectivity based on the IC_{50} values of PTX delivery reveals an increase in selectivity from ca. 1.26 for free PTX to ca. 1.76 for PTX@NanoMUV-2.

Surface modifications of NanoMUV-2

Given these encouraging results, we functionalized the surface of NanoMUV-2 samples with the aim to tune its degradation and drug release kinetics as well as increasing cell internalization and selectivity through fine-tuning of the cellular internalization routes.[42] For this purpose, we have chosen 8-Br octanoic acid (Oct) and folic acid (FA) as surface coatings, both containing carboxylate groups for attachment leading to NanoMUV-2-Oct and NanoMUV-2-FA, respectively. On the one hand, alkanes are highly hydrophobic and thus shall promote cell permeation.[43] Folic acid, on the other hand, is hydrophilic, but it is known for its cancer-targeting effect since cancer cells typically over-express the folate receptor,[44] and it is also established to tune internalization pathways towards more efficient cytosol delivery.[9]

NanoMUV-2 retains its crystalline structure after both surface coatings (see section S9 in the ESI†). Importantly, FT-IR and TGA revealed the successful attachment of both surface coatings, whereas different characterisation techniques such as Energy-Dispersive X-Ray (EDX), Proton Nuclear Magnetic Resonance (^{1}H NMR), and TGA[41] confirmed similar weight per cent for both coatings, 11.8 ± 0.8% w/w of Oct on

This journal is © The Royal Society of Chemistry 2023

J. Mater. Chem. B, 2023, 11, 9179–9184 | 9181

Fig. 4 (a) Linker release from functionalized and uncoated NanoMUV-2 in PBS 10X. (b) HeLa and HEK cells' viability upon incubation with different concentrations of functionalized NanoMUV-2. Error bars represent the standard deviation of 3 independent experiments, each of them with $n = 4$.

NanoMUV-2-Oct and $8.9 \pm 0.1\%$ w/w of FA on NanoMUV-2-FA. N_2 sorption studies suggested inner and outer surface coating, which is expected due to the large, accessible pores of MUV-2. The great colloidal stability of uncoated NanoMUV-2 in PBS 10X, was maintained for NanoMUV-2-Oct and further enhanced upon FA coating. Partial pore blockage by the surface coatings slows the degradation kinetics in PBS 10X due to the formation of a phosphate corona (Fig. S66 and S80, ESI†) that prevents further degradation,[3] leading to a maximum of ca. 40% linker release for the hydrophobic-coated NanoMUV-2-Oct after 8 hours and to a maximum of ca. 70% linker release in the case of the hydrophilic NanoMUV-2-FA, as represented in Fig. 4a.

NanoMUV-2-Oct and NanoMUV-2-FA displayed a decrease in cell proliferation compared to the precursor NanoMUV-2 (Fig. 4b), which aligns with the cytotoxicity of the free ligand salt (see section S10 in the ESI†) and hence suggests higher cell internalization and/or more efficient cellular uptake routes towards cytosol delivery. The associated cytotoxicity was in general more pronounced for HeLa cervix cancer cells, and, nevertheless, none of the MOFs had a negative effect on cell proliferation up to 0.3 mg mL^{-1}, whereas, at this concentration of PTX@NanoMUV-2, there is negligible cell viability for both cell lines.

Effect of surface modifications on selective PTX delivery

To evaluate the effect of surface coatings on cell internalization efficiency and selectivity, as well as on drug release kinetics, we coated Cal@NanoMUV-2 leading to Cal@NanoMUV-2-Oct and Cal@NanoMUV-2-FA (see section S11 in the ESI†). Full characterisation confirms structural integrity and successful surface coating attachment and like the effect on degradation kinetics, the surface modifications led to the formation of a phosphate corona through partial pore blockage, which hindered further drug release after ca. 60% calcein release up to 3 hours.

Flow-assisted cell cytometry confirmed efficient calcein delivery into cells by the surface-modified drug delivery systems (see section S12.1 in the ESI†). Both surface coatings enhanced internalization by HeLa cells, with no statistical significance

Fig. 5 (a) Endocytosis efficiency of calcein-loaded MOFs. Cytoplasmic fluorescence was normalized towards Cal@NanoMUV-2 at 0.5 mg mL^{-1} concentration for HeLa cells. (b) Endocytosis efficiency of functionalized NanoMUV-2 compared to uncoated NanoMUV-2 and free calcein. Cytoplasmic fluorescence was normalized towards the untreated controls (as a fold increase). Error bars represent the standard deviation of 3 independent experiments. (c) Confocal microscopy images of HeLa cells upon treatment with 0.2 mg mL^{-1} of calcein-loaded MOFs for 2 hours. (d) Confocal microscopy colocalization studies upon treatment with 0.05 mg mL^{-1} for 2 hours (right HeLa cells, left HEK cells). (e) Manders' correlation coefficients extracted from colocalization studies. Error bars correspond to the standard deviation of 5 independent images.

9182 | J. Mater. Chem. B, 2023, 11, 9179–9184

This journal is © The Royal Society of Chemistry 2023

between the coated MOFs among high concentrations (Fig. 5a). However, the internalization of Cal@NanoMUV-2FA was more significant at low concentrations (0.005 and 0.05 mg mL^{-1} of MOF), with a *ca.* 13-fold increase compared to Cal@NanoMUV-2, whereas a *ca.* 3-fold increase was observed for Cal@Nano-MUV-2-Oct, considering in both cases the calcein loading of the systems. For higher concentrations, the enhancement compared to Cal@NanoMUV-2 ranged from *ca.* 1.5 to 2-fold increase for both surface-coated MOFs.

The hydrophobic Cal@NanoMUV-2-Oct was less selective for HeLa cells than the hydrophilic Cal@NanoMUV-2-FA, observing for the later a reduced uptake for non-targeted HEK cells, more pronounced at higher concentrations (Fig. 5a). This explains the differences in the selective cytotoxicity of the surface-modified samples, with more cancer-selective internalization for Cal@Na-noMUV-2-FA leading to more selective cytotoxicity. As cell internalization is enhanced for both HeLa and HEK cells in the case of Cal@NanoMUV-2-Oct, the cytotoxicity of NanoMUV-2-Oct towards both cell lines is more similar.

Confocal microscopy of HeLa Cells upon incubation with 0.2 mg mL^{-1} dispersions of MOFs for 2 hours agreed with the results obtained through FACS, showing an enhancement in the internalization of calcein (Fig. 5b). Moreover, more diffuse patterns of calcein were observed (Fig. 5c), suggesting efficient cytosol delivery and less endosome/lysosome trapping. This was confirmed by colocalisation studies using Lysotracker (Fig. 5d). HeLa cells showed a decrease in colocalized calcein, with diffusion patterns across the cytosol, whereas, in the case of HEK cells, the co-localization was similar, as represented by the differences in Manders' coefficients (Fig. 5e) (see section S12.2 in the ESI†).

Surface modifications were performed on PTX@NanoMUV-2 following similar procedures and optimal surface coating was confirmed by a number of techniques including ^{1}H NMR, FT-IR, EDX and TGA among others, leading to PTX@NanoMUV-2-Oct and PTX@NanoMUV-2-FA with minimum PTX leaching (see section S13 in the ESI†). The effect of the coated PTX@MOF systems on cell proliferation was in agreement with the increase in internalization efficiency and cytosol delivery evaluated on the coated Cal@NanoMUV-2 analogues for HeLa cells (see section S14 in the ESI†).

Comparing the effect on cell proliferation of the three PTX-loaded MOFs as a function of the maximum concentration of PTX that could be delivered (Fig. 6a) reveals an increase in the cytotoxicity towards HeLa cells for both coated MOFs, possibly given that both systems can scape lysosome formation, leading to efficient cytosol delivery. As a result, the proposed NanoMUV-2 formulations reach similar PTX therapeutic effects in HeLa cells as compared to free PTX.

The cytotoxicity towards HEK cells was slightly reduced, possibly due to the reduced lysosomal scape for HEK cells. Thus, the anticancer selectivity of the drug-loaded materials based on the determined IC$_{50}$ values (Fig. 6b) was increased from *ca.* 1.3 for free PTX and *ca.* 1.7 for PTX@NanoMUV-2, to *ca.* 8 for the surface-coated materials, suggesting that efficient cytosol delivery plays a more important role than selective internalisation.

Fig. 6 (a) HeLa and HEK normalized cell viability upon incubation with different concentrations of PTX@NanoMUV-2, PTX@NanoMUV-2-Oct and PTX@NanoMUV-2-FA as a function of the maximum concentration of PTX reached upon total delivery, in comparison with PTX@NanoMUV-2. (b) IC$_{50}$ values of the different PTX-loaded MOFs in comparison with free PTX.

Conclusions

In conclusion, we have assessed the suitability of the meso-porous NanoMUV-2 for drug delivery applications, presenting a synthetic route to obtain nanoparticles. NanoMUV-2 exhibits optimal colloidal stability, great biocompatibility (with IC$_{50}$ of *ca.* 1.9 mg mL^{-1}), fast degradation kinetics that shall avoid accumulation in the body, and is internalized by cells.

The superior pore size and opening of MUV-2 allows significant pore loading of big biomolecules such as PTX (*ca.* 22% w/w), one of the most widely applied chemotherapeutics. Moreover, NanoMUV-2 has been proven to be versatile for surface modifications, which further enhance its colloidal stability, chemical stability towards degradation and drug release kinetics as well as cell permeation, efficient cytosol delivery and cancer targeting effects. Ultimately, we have shown that surface functionalization greatly enhanced PTX selectivity, opening the door for PTX resistance studies.

Conflicts of interest

There are no conflicts to declare.

Acknowledgements

References

1 H.-C. Joe Zhou and S. Kitagawa, *Chem. Soc. Rev.*, 2014, **43**, 5415–5418.

2 C. G. Piscopo and S. Loebbecke, *ChemPlusChem*, 2020, **85**, 538–547.

This journal is © The Royal Society of Chemistry 2023

J. Mater. Chem. B, 2023, **11**, 9179–9184 | 9183

3 I. Abánades Lázaro and R. S. Forgan, *Coord. Chem. Rev.*, 2019, **380**, 230–259.

4 M. Giménez-Marqués, T. Hidalgo, C. Serre and P. Horcajada, *Coord. Chem. Rev.*, 2016, **307**, 342–360.

5 P. Horcajada, T. Chalati, C. Serre, B. Gillet, C. Sebrie, T. Baati, J. F. Eubank, D. Heurtaux, P. Clayette, C. Kreuz, J.-S. Chang, Y. K. Hwang, V. Marsaud, P.-N. Bories, L. Cynober, S. Gil, G. Férey, P. Couvreur and R. Gref, *Nat. Mater.*, 2010, **9**, 172–178.

6 S. Haddad, I. Abánades Lázaro, M. Fantham, A. Mishra, J. Silvestre-Albero, J. W. M. Osterrieth, G. S. K. Schierle, C. F. Kaminski, R. S. Forgan and D. Fairen-Jimenez, *J. Am. Chem. Soc.*, 2020, **142**, 6661–6674.

7 M. H. Teplensky, M. Fantham, P. Li, T. C. Wang, J. P. Mehta, L. J. Young, P. Z. Moghadam, J. T. Hupp, O. K. Farha, C. F. Kaminski and D. Fairen-Jimenez, *J. Am. Chem. Soc.*, 2017, **139**, 7522–7532.

8 I. Abánades Lázaro, C. J. R. Wells and R. S. Forgan, *Angew. Chem., Int. Ed.*, 2020, **59**, 5211–5217.

9 I. Abánades Lázaro, S. Haddad, J. M. Rodrigo-Muñoz, C. Orellana-Tavra, V. del Pozo, D. Fairen-Jimenez and R. S. Forgan, *ACS Appl. Mater. Interfaces*, 2018, **10**, 5255–5268.

10 R. Röder, T. Preiß, P. Hirschle, B. Steinborn, A. Zimpel, M. Höhn, J. O. Rädler, T. Bein, E. Wagner, S. Wuttke and U. Lächelt, *J. Am. Chem. Soc.*, 2017, **139**, 2359–2368.

11 S. Nagata, K. Kokado and K. Sada, *Chem. Commun.*, 2015, **51**, 8614–8617.

12 W.-H. Chen, X. Yu, A. Cecconello, Y. S. Sohn, R. Nechushtai and I. Willner, *Chem. Sci.*, 2017, **8**, 5769–5780.

13 K. M. L. Taylor-Pashow, J. D. Rocca, Z. Xie, S. Tran and W. Lin, *J. Am. Chem. Soc.*, 2009, **131**, 14261.

14 S. Sene, M. T. Marcos-Almaraz, N. Menguy, J. Scola, J. Volatron, R. Rouland, J.-M. Grenèche, S. Miraux, C. Menet, N. Guillou, F. Gazeau, C. Serre, P. Horcajada and N. Steunou, *Chem*, 2017, **3**, 303–322.

15 C. Tamames-Tabar, D. Cunha, E. Imbuluzqueta, F. Ragone, C. Serre, M. J. Blanco-Prieto and P. Horcajada, *J. Mater. Chem. B*, 2013, **2**, 262–271.

16 T. Hidalgo, R. Simón-Vázquez, A. González-Fernández and P. Horcajada, *Chem. Sci.*, 2021, **13**, 934–944.

17 I. Abánades Lázaro, J. M. Rodrigo-Muñoz, B. Sastre, M. R. Ángel, C. Martí-Gastaldo and V. del Pozo, *J. Mater. Chem. B*, 2021, **9**, 6144–6148.

18 J. C. Diaz, B. Lozano-Torres and M. Gimenez-Marques, *Chem. Mater.*, 2022, **34**, 7817–7827.

19 L. O. Alimi, M. Z. Alyami, S. Chand, W. Baslyman and N. M. Khashab, *Chem. Sci.*, 2021, **12**, 2329–2344.

20 M. A. Jordan and L. Wilson, *Nat. Rev. Cancer*, 2004, **4**, 253–265.

21 H. Gelderblom, J. Verweij, K. Nooter and A. Sparreboom, *Eur. J. Cancer*, 2001, **37**, 1590–1598.

22 P. Ma and R. J. Mumper, *J. Nanomed. Nanotechnol.*, 2013, **04**, 1000164.

23 M. J. Hawkins, P. Soon-Shiong and N. Desai, *Adv. Drug Delivery Rev.*, 2008, **60**, 876–885.

24 A. Ma and R. Zhang, *Mater. Res. Exp.*, 2020, **7**, 095402.

25 A. Bazzazzadeh, B. F. Dizaji, N. Kianinejad, A. Nouri and M. Irani, *Int. J. Pharm.*, 2020, **587**, 119674.

26 N. D. Bikiaris, N. M. Ainali, E. Christodoulou, M. Kostoglou, T. Kehagias, E. Papasouli, E. N. Koukaras and S. G. Nanaki, *Nanomaterials*, 2020, **10**, 2490–2520.

27 F. Ge, R. Qiao, P. Song, Y. Tao, L. Zhu, W. Zhang, W. Li and L. Gui, *Mater. Res. Express*, 2021, **8**, 045012.

28 M. Filippousi, S. Turner, K. Leus, P. I. Siafaka, E. D. Tseligka, M. Vandichel, S. G. Nanaki, I. S. Vizirianakis, D. N. Bikiaris, P. V. D. Voort and G. V. Tendeloo, *Int. J. Pharm.*, 2016, **509**, 208–218.

29 L. H. T. Nguyen, Y. T. Dang, T. T. T. Nguyen, B. Q. G. Le, N. X. D. Mai, H. V. Nguyen, M.-T. Le, T. B. Phan and T. L. H. Doan, *New J. Chem.*, 2022, **46**, 6630–6635.

30 K. Hamidian, M. Barani, M. Adeli-Sardou, M. Sarani, S. Daliran and A. R. Oveisi, *Heliyon*, 2023, **9**, e12634.

31 M. Souto, A. Santiago-Portillo, M. Palomino, I. J. Vitórica-Yrezábal, B. J. C. Vieira, J. C. Waerenborgh, S. Valencia, S. Navalón, F. Rey, H. García and G. Mínguez Espallargas, *Chem. Sci.*, 2018, **9**, 2413–2418.

32 M. Souto, J. Romero, J. Calbo, I. J. Vitórica-Yrezábal, J. L. Zafra, J. Casado, E. Ortí, A. Walsh and G. Mínguez Espallargas, *J. Am. Chem. Soc.*, 2018, **140**, 10562.

33 M. Vicent-Morales, I. J. Vitórica-Yrezábal, M. Souto and G. Mínguez Espallargas, *CrystEngComm*, 2019, **21**, 3031–3035.

34 C. R. Marshall, S. A. Staudhammer and C. K. Brozek, *Chem. Sci.*, 2019, **10**, 9396–9408.

35 S. Krause, V. Bon, I. Senkovska, D. M. Többens, D. Wallacher, R. S. Pillai, G. Maurin and S. Kaskel, *Nat. Commun.*, 2018, **9**, 1573–1581.

36 E. Bellido, T. Hidalgo, M. V. Lozano, M. Guillevic, R. Simón-Vázquez, M. J. Santander-Ortega, Á. González-Fernández, C. Serre, M. J. Alonso and P. Horcajada, *Adv. Healthcare Mater.*, 2015, **4**, 1246–1257.

37 C. Orellana-Tavra, R. J. Marshall, E. F. Baxter, I. Abánades Lázaro, A. Tao, A. K. Cheetham, R. S. Forgan and D. Fairen-Jimenez, *J. Mater. Chem. B*, 2016, **4**, 7697–7707.

38 C. Orellana-Tavra, E. F. Baxter, T. Tian, T. D. Bennett, N. K. H. Slater, A. K. Cheetham and D. Fairen-Jimenez, *Chem. Commun.*, 2015, **51**, 13878.

39 W. D. Stein and T. Litman, *Primary active transport systems*, Channels, carriers, and pumps, Elsevier, London, United Kingdom, 2nd edn, 2015, ch. 6, pp. 247–328.

40 L. Kou, J. Sun, Y. Zhai and Z. He, *Asian J. Pharm. Sci.*, 2013, **8**, 1–10.

41 I. Abánades Lázaro, *Eur. J. Inorg. Chem.*, 2020, 4284–4294.

42 M. S. de Almeida, E. Susnik, B. Drasler, P. Taladriz-Blanco, A. Petri-Fink and B. Rothen-Rutishauser, *Chem. Soc. Rev.*, 2021, **50**, 5397–5434.

43 C. M. Backlund, F. Sgolastra, R. Otter, L. M. Minter, T. Takeuchi, S. Futaki and G. N. Tew, *Polym. Chem.*, 2016, **7**, 7514–7521.

44 G. L. Zwicke, G. A. Mansoori and C. J. Jeffery, *Nano Rev.*, 2012, **3**, 18496.

9184 | *J. Mater. Chem. B*, 2023, **11**, 9179–9184

This journal is © The Royal Society of Chemistry 2023